Longitudinal four-dimensional mapping of subcortical anatomy in human development

Armin Raznahan[a,1], Phillip W. Shaw[b], Jason P. Lerch[c], Liv S. Clasen[a], Deanna Greenstein[a], Rebecca Berman[a], Jon Pipitone[d], Mallar M. Chakravarty[c,d,e,2], and Jay N. Giedd[a,2]

[a]Child Psychiatry Branch, National Institute of Mental Health, Bethesda, MD 20892; [b]Neurobehavioral Clinical Research Section, Social and Behavioral Research Branch, National Human Genome Research Institute, National Institutes of Health, Bethesda, MD 20892; [c]Kimel Family Imaging-Genetic Research Laboratory, Centre for Addiction and Mental Health, Toronto, ON, Canada M5T 1R8; [d]Department of Psychiatry and Institute of Biomaterials and Biomedical Engineering, University of Toronto, Toronto, ON, Canada M5T 1R8; and [e]Rotman Research Institute, Toronto, ON, Canada M6A 2E1

Edited by Marcus E. Raichle, Washington University, St. Louis, MO, and approved December 11, 2013 (received for review September 9, 2013)

Growing access to large-scale longitudinal structural neuroimaging data has fundamentally altered our understanding of cortical development en route to human adulthood, with consequences for basic science, medicine, and public policy. In striking contrast, basic anatomical development of subcortical structures such as the striatum, pallidum, and thalamus has remained poorly described—despite these evolutionarily ancient structures being both intimate working partners of the cortical sheet and critical to diverse developmentally emergent skills and disorders. Here, to begin addressing this disparity, we apply methods for the measurement of subcortical volume and shape to 1,171 longitudinally acquired structural magnetic resonance imaging brain scans from 618 typically developing males and females aged 5–25 y. We show that the striatum, pallidum, and thalamus each follow curvilinear trajectories of volume change, which, for the striatum and thalamus, peak after cortical volume has already begun to decline and show a relative delay in males. Four-dimensional mapping of subcortical shape reveals that (*i*) striatal, pallidal, and thalamic domains linked to specific fronto-parietal association cortices contract with age whereas other subcortical territories expand, and (*ii*) each structure harbors hotspots of sexually dimorphic change over adolescence—with relevance for sex-biased mental disorders emerging in youth. By establishing the developmental dynamism, spatial heterochronicity, and sexual dimorphism of human subcortical maturation, these data bring our spatiotemporal understanding of subcortical development closer to that of the cortex—allowing evolutionary, basic, and clinical neuroscience to be conducted within a more comprehensive developmental framework.

Our understanding of human brain maturation has been rapidly advanced over the past decade by increased availability of large longitudinal in vivo structural magnetic resonance imaging (sMRI) datasets of pediatric brain development (1). However, to date, large-scale longitudinal sMRI studies have focused on the cortical sheet at the expense of subcortical structures such as the striatum, pallidum, and thalamus. Through the analysis of such data, we now know that cortical volume does not undergo a spatially homogenous linear change with development, but rather follows a highly dynamic and regionally heterogenous "inverted-U" trajectory (2–5). These basic aspects of anatomical maturation—the timing of overall growth and regional differences in the tempo of structural maturation—have yet to be longitudinally resolved in the human subcortex (6–9).

Access to spatiotemporally fine-grained maps of human cortical development has had major scientific and societal consequences. These maps have impacted the study of brain evolution (10), cognitive–behavioral variation in health (11), and mechanisms of neurodevelopmental disease (12, 13). However, evolution, function, and dysfunction of the cortical sheet occur in the context of its rich structural and functional connectedness with the subcortex, and vice versa (14, 15). Therefore, there is a pressing need to equilibrate our understanding of cortical and subcortical maturation—to obtain a more spatially comprehensive model of human brain development.

Here, we apply methods for sMRI analysis of striatal, pallidal, and thalamic anatomy (16, 17) to one of the largest existing longitudinal datasets of pediatric brain development (18). Our methods estimate the overall volume of each structure, as well as local surface area at a total of ~20,000 points (vertices), making it possible to resolve focal alterations in subcortical shape, which can occur in the absence of changes in overall volume. Because our methods are built upon classical atlases of serial subcortical histology (19–21), we can align spatially fine-grained in vivo imaging findings with microscopic subcortical distinctions.

We first seek to clarify whether gross volumetric development of the striatum, pallidum, and thalamus follows curvilinear trajectories akin to those reported for the cortical sheet (2). Resolving curvilinear anatomical change makes it possible to time specific maturational milestones—such as age at attainment of peak size—which can serve as markers for the definition of developmental sequences (13). These sequences may carry evolutionary and functional significance: Within the cortex, structures that are last to reach their peak size tend to be those that have undergone preferential expansion in primates and that are involved in complex, integrative and late-maturing cognitive functions (22–24). With this framework in mind, we determine the developmental ordering of different subcortical structures relative to each other and the cortex. Clarifying this ordering could inform cognitive neuroscience models that consider developmental

Significance

Our spatiotemporal understanding of subcortical development in humans lags far behind that of the cortical sheet. This disparity ignores that developmental refinements and disruptions of complex behavior involve systems spanning both components of the brain. We begin redressing this imbalance by applying new techniques for striatal, pallidal and thalamic morphometry to large-scale longitudinal neuroimaging data extending from childhood through early adulthood. This work (*i*) establishes the curvilinear, sexual dimorphic and often protracted nature of global volume change within each structure, (*ii*) reveals profound spatiotemporal complexities in striatal, pallidal and thalamic maturation that are organized by the known topography of primate cortico-subcortical connectivity, and (*iii*) identifies focal sex differences in subcortical maturation that strike regions implicated in psychopathologies with an adolescent-emergent sex-bias.

Author contributions: A.R. and J.N.G. designed research; A.R., P.W.S., L.S.C., D.G., R.B., and M.M.C. performed research; J.P.L., J.P., and M.M.C. contributed new reagents/analytic tools; A.R. analyzed data; and A.R. wrote the paper.

The authors declare no conflict of interest.

This article is a PNAS Direct Submission.

[1]To whom correspondence should be addressed. E-mail: raznahana@mail.nih.gov.

[2]M.M.C. and J.N.G. contributed equally to this work.

This article contains supporting information online at www.pnas.org/lookup/suppl/doi:10.1073/pnas.1316911111/-/DCSupplemental.

balances between maturing prefrontal "control" systems and striatal "motivational" centers as being pivotal to adolescent increases in risk-taking behavior (25, 26).

Next, we longitudinally map regional variation in rates of anatomical change within each subcortical structure by analyzing trajectories of local surface area change. Existing descriptions of subcortical connectivity in primates and humans provide an important context for the study of spatial differences in the tempo of subcortical maturation (27). The striatum, pallidum, and thalamus are linked with each other and the cortical sheet through a series of topographically organized cortico-basal ganglia-thalamo-cortical "loops" (28), which subserve partly distinct affective, cognitive, and sensorimotor functions (29). Although there are rich structural and functional interactions between these loops (28, 30, 31), their topography can be defined in terms of stereotypic projection fields between different components of the cortex, striatum, pallidum, and thalamus (29). Human neuroimaging data suggest that these stereotypic projection fields organize concordant spatial patterns of brain activity across different level of the cortico-basal ganglia-thalamo-cortical system (30, 32). We harness our spatially fine-grained map of striatal, pallidal, and thalamic maturation to ask whether known spatial differences in the tempo of cortical maturation (5, 22) are mirrored by spatial differences in subcortical maturation that respect the topography of cortico-basal ganglia-thalamo-cortical loops.

Finally, building on prominent longitudinal reports of sex differences in the tempo of pediatric cortical maturation (33, 34), we quantify sex differences in global and local subcortical maturation between childhood and early adulthood. Clarifying the nature of sexually dimorphic subcortical maturation during this developmental window is especially important given that (*i*) males and females diverge in risk affective disorders (female bias) and antisocial behaviors (male bias) (35, 36) during adolescence, and (*ii*) subcortical structures are known to play a key role in adaptive and disordered regulation of affect (37, 38) and motivated behavior (39, 40).

Results

Participant Characteristics (Table S1). We included 1,172 longitudinally acquired sMRI brain scans from 618 youth (306 female, 312 male) aged 5 through 25 y (see Fig. S1 for age distribution). Of all 618 participants with at least 1 brain sMRI scan, 55% had 2 or more and 24% had 3 or more scans. Scans were acquired at ∼2-y intervals using the same 1.5-T General Electric Signa scanner.

Trajectories of Subcortical Volume Development Are Curvilinear and Differ by Structure and Sex. Fig. 1 shows raw person-level and estimated group-level developmental trajectories for bilateral striatal, pallidal, thalamic, and cortical volume. Fig. S2 shows the derivatives of these volume-by-age curves for each structure—separately for males and females. Table S2 contains test statistics and associated *P* values from the mixed-effects models used to define these trajectories (*Methods*). At the group level, all three structures show significantly cubic developmental trajectories ($P < 0.0001$ for striatum and thalamus, $P < 0.0004$ for pallidum) and significantly greater absolute volumes in males than females throughout the age range examined ($P < 0.0005$). For each structure volume trajectories are significantly different between males and females ($P < 0.0001$ for striatum and thalamus, $P = 0.05$ for pallidum). Males attain peak striatal and thalamic volume significantly later than females (Table 1). In both sexes, the pallidum is first to peak in volume, followed by the striatum and the thalamus [95% confidence intervals (CI) nonoverlapping for females], and the striatum and thalamus reached peak volume later than the cortical sheet. In preliminary analyses of the relationship between IQ and interindividual variation in subcortical anatomy, we found statistically significant positive relationships between IQ and the volume of all three structures examined although these relationships were no longer present after covarying for total brain volume (Table S3).

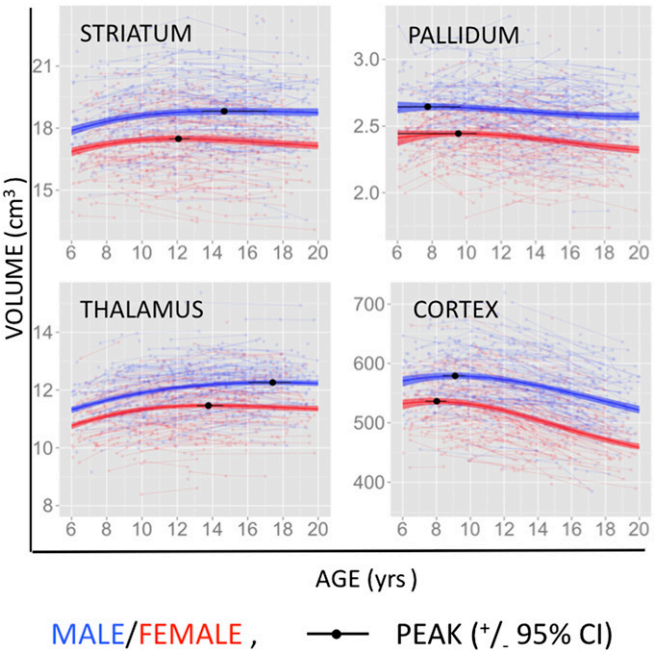

Fig. 1. Developmental trajectories for global volume. Plots showing individual level anatomical data and best-fit group-level trajectories for bilateral striatal, pallidal, and thalamic volume. Shaded ribbons around each curve denote 95% confidence intervals.

Subcortical Development Is Highly Heterochronous. Our data indicate that local rates of anatomical change vary greatly within each subcortical structure examined. Fig. 2 shows an unthresholded map for the annual rate of local ("vertex-level") surface area change in each subcortical structure (Fig. 2*A*). Thresholded versions of these maps using false discovery rate (FDR) correction for multiple comparison (with *q* set at 0.05) (41) are provided in Fig. 2.

Striatal area expansion with age is most evident in the caudate tail and caudolateral putamen bilaterally. Facets of striatal contraction are predominantly localized to rostro-ventral regions of the caudate and putamen. The pallidum also shows a prominent rostral bias toward areal contraction: Although the rostral pallidum contracts with advancing age, the caudal pallidum expands. The thalamus shows a widespread pattern of age-related areal expansion (fastest at ventral and dorsal thalamic extremities), which is punctuated by three bilateral, symmetric, and well-circumscribed regions of developmental thalamic contraction that are located on dorsomedial, anteriolateral, and opposing medial thalamic facets. Comparison with histologically defined

Table 1. Estimated age at which each structure examined attains peak volume in males and females

	Peak volume females		Peak volume males	
Structure	Age	95% CI	Age	95% CI
Striatum	12.1	11.5–12.7	14.7	13.4–17.1
Pallidum	9.5	6.9–10.6	7.7	2–9.6
Thalamus	13.8	13.1–14.6	17.4	16.0–18.5
Cortex	8.0	7.35–8.59	9.1	8.37–9.68

The estimated peak age and 95% confidence intervals were derived by bootstrapping methods involving repeat modeling of curvilinear growth in 1,000 samples—constructed by sampling with replacement.

NEUROSCIENCE

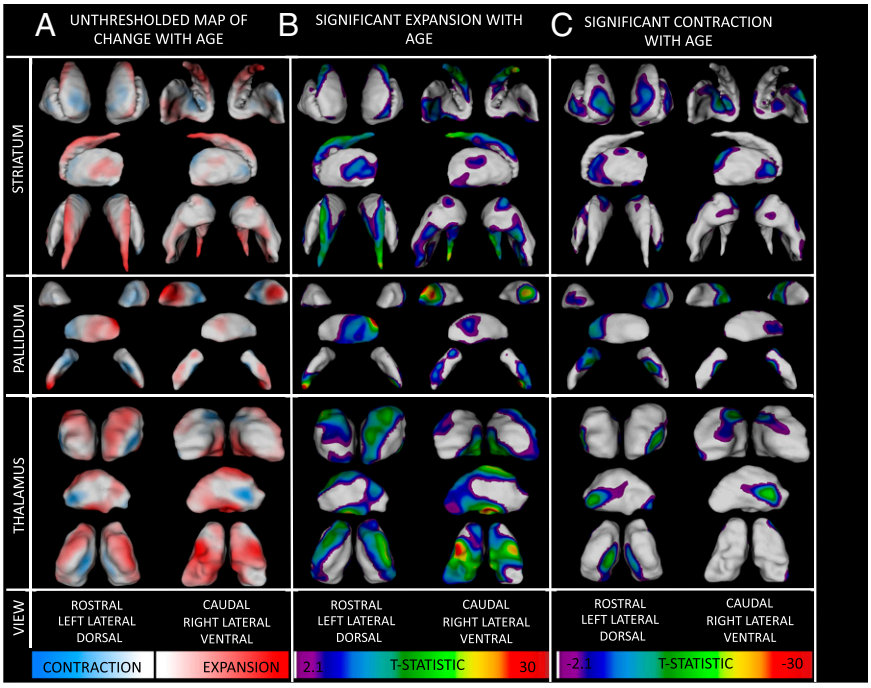

Fig. 2. Maps of age-related expansion and contraction. (*A*) Unthresholded maps where color encodes regional differences in the direction (blue, contraction; red, expansion) and rate (greater saturation, faster change) of linear surface-area change with increasing age. (*B*) Colored regions denote significant areal expansion with age after FDR correction for multiple comparisons. Warmer colors denote more pronounced linear expansion with age. (*C*) Colored regions denote significant areal contraction with age after FDR correction for multiple comparisons. Warmer colors denote more pronounced linear contraction with age.

surface labels for thalamic subnuclei (Fig. S3) indicates that regions of thalamic contraction overlie ventral anterior (VA), rostral ventrolateral (VL), and mediodorsal (MD) nuclei. Movie S1 assembles the left thalamus, pallidum, and striatum in anatomical space to highlight the close alignment between facets of areal contraction in different structures. Movie S2 tracks the evolution of local subcortical contraction and expansion with advancing age.

Localizing Hotspots of Sexually Dimorphic Subcortical Maturation. Fig. 3 provides a spatially fine-grained map of sexually dimorphic subcortical maturation between childhood and early adulthood. At all regions where rates of anatomical change differ between males and females, males begin with larger local surface area than females and become more dissimilar from females during the adolescent transition into early adulthood. However, this phenomenon is driven by a different effect in each of the three subcortical structures examined (see inset plots in Fig. 3): In striatal foci, there is a lack of significant age-related anatomical change in females alongside significant age-related areal expansion in males; in pallidal foci, there is an absence of significant age-related anatomical change in males alongside significant age-related areal contraction in females and, in the thalamus, significant age-related expansion is seen in both sexes although the rate of change is faster in males than females. Across all three structures examined, sex differences in subcortical maturation tend to be ventrally rather than rostrally localized and are bilaterally symmetric (with the exception of left rostro-caudal and right ventro-caudal putamen). Comparison with histologically defined surface labels within the thalamus localizes foci of sexually dimorphic maturation to bilateral centromedial (CMed), ventromedial putamen, caudal lateral posterior (LP) and anterior group (Ant) nuclei, as well as caudal portions of the right MD nucleus.

Discussion

Gross Volumetric Development. Volumetric development of all three subcortical structures examined is considerably more curvilinear and sexually dimorphic than had been suggested by previous studies using smaller cross-sectional sMRI datsets (8, 9). Males and females show significant differences in both absolute subcortical volume and the timing of developmental changes in subcortical volume. The significant subcortical volumetric sex differences that we identify during prepubertal life are necessarily independent of pubertally emergent sex differences in circulating gonadal sex steroid levels. However, our data hint that pubertal timing in males and females may influence trajectories of subcortical volume change, because (*i*) the relative delay in male attainment of peak striatal and thalamic volume echoes the relative male delay in the onset of puberty-associated somatic growth spurt (42) and (*ii*) rates of annual striatal, pallidal, and thalamic volume loss in both sexes approach zero [i.e., volume curves "plateau" (Fig. S2)] when maturation of secondary sexual characteristics is typically completed (43, 44).

For both males and females, striatal and thalamic maturation—as indexed by age at attainment of peak volume—is protracted relative to total cortical volume maturation. Protracted volumetric maturation within the brain has been apportioned evolutionary and functional significance based on findings within the cortical sheet: Later-maturing cortical regions tend to be those that have also undergone more pronounced evolutionary expansion [as inferred from comparisons between adult humans and nonhuman primates (5, 10, 22)] and show stronger links with higher order cognition vs. sensorimotor processing (5, 22). Our findings indicate that these evolutionary and functional corollaries of protracted volumetric maturation do not necessarily generalize outside the cortical sheet: The striatum and thalamus show protracted maturation relative to the cortical sheet, but less evolutionary expansion in absolute size based on cross-species comparisons (45), and less specific associations with higher cognition (46). Protracted maturation of the striatum relative to the cortical sheet is also surprising when considered in light of the prominent "Dual Systems" model for adolescent increases in risk-taking behavior, which posits a protraction in cortical maturation relative to the striatum (25, 26). These discords draw attention to two challenges in the definition of developmental sequences within the brain using tempos of volumetric maturation. First, the order with which different gray matter structures attain peak volume may be influenced by interstructure differences in tissue composition. For example, knowing that myelin-rich white matter components of the brain continue to increase in volume long after myelin-poor gray matter components have already started to decline in volume (8, 23) suggests that notably late attainment of

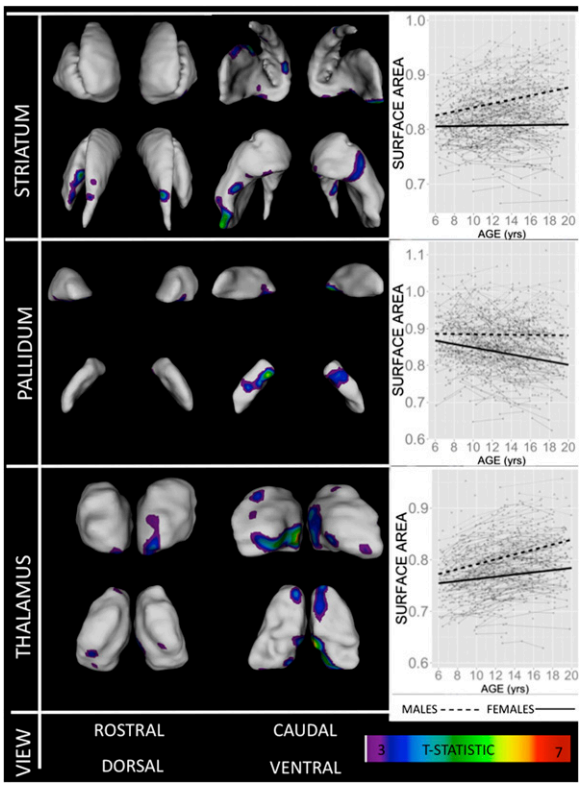

Fig. 3. Hotspots of sexually dimorphic subcortical maturation. Colored regions show foci of significant (after FDR correction with q set at 0.05) male–female differences in the rate of local areal change between childhood and early adulthood. Warmer colors denote more pronounced differences. *Inset* plots for each structure show individual level anatomical data and best-fit group level trajectories for mean surface area within regions of sexually dimorphic maturation in each sex.

peak thalamic volume could be driven by the significant fraction of total thalamic volume that contains myelinated fibers (21). Second, developmental ordering may vary according to the developmental milestone selected. Although attention has focused on attainment of peak volume, other metrics—such as age at maximal volume change—are equally valid but largely unexplored "stopwatches" for the maturing brain.

Regionally Heterochronous Development. Different regions within each subcortical structure can show profound differences in their anatomical change with age: Some subcortical regions contract with advancing age whereas others expand. Thus, as for the cortical sheet (5, 22), subcortical structural development is regionally heterogeneous. This finding underlines the importance of using methods that allow detailed consideration of subregional anatomy in future studies of subcortical variability during typical and atypical development. Moreover, there is a striking conformity between our maturational division of subcortical territories and the topography of cortico-basal ganglia-thalamo-cortical circuitry charted by tract-tracing studies in nonhuman primates (47–50) and neuroimaging studies of functional (30, 51) and white-matter connectivity (32, 52, 53) in humans.

The predominantly ventro-rostral region of striatal contraction is known to preferentially receive inputs from ventromedial vs. caudolateral prefrontal cortices (27, 30, 47) and rostral vs. caudal insula (54). These ventro-rostral regions of striatal contraction are in turn known to project onto rostral territories of the pallidum (49, 55, 56), which constitute the main foci of pallidal contraction in our study. Thus, pallidal maturation appears to be organized by rostro-caudal and medio-lateral gradients of striato-pallidal connectivity, which cut-across external and internal pallidal segments (56). Our thalamic findings further reinforce the coherence between subcortical maturation and connectivity. Specifically, primate tract-tracing studies have established preferential connectivity between the rostro-ventral striatum/pallidum and those thalamic subnuclei that constitute domains of contraction within our study [rostro-ventral striatum–ventral anterior (VA), medio-dorsal (MD), and midline thalamic nuclei (48, 57), rostral pallidum-VA thalamus (58, 59)]. These thalamic subnuclei are in turn richly interconnected with cortical regions that send efferents to the rostro-ventral striatum [prefrontal (50, 60, 61), insular (60), and superior parietal cortex (62, 63)]. Thus, our data suggest that striato-pallido-thalamic components that are preferentially linked to rostral prefrontal and superior parietal association cortices contract over development whereas those more strongly associated with caudolateral prefrontal, primary sensorimotor (64), posteriomedial (65, 66), inferior parietal, occipital, and inferior temporal cortices (67, 68) tend to expand.

The aligment of subcortical maturation with known patterns of subcortical connectivity strongly suggests that developmental changes in local surface area reflect changes in underlying subcortical parenchyma. Speculatively, these changes may reflect developmental modification of dendritic, neuropil, axonal, or myelin compartments within the subcortex, but histological data in primates are scarce (69). Local changes in subcortical shape could also reflect processes in overlying white-matter tracts (70) such as rostral external capsule, inferior fronto-occipital fasciculus (over latero-rostral facets of putamen and caudate), anterior limb of the internal capsule and anterior commissure (over rostromedial facets of putamen and caudate), and genu of internal capsule (over VA thalamus). However, this alternative hypothesis is weakened by evidence that white matter surrounding deep structures undergoes robust developmental expansion (71).

Sexually Dimorphic Development. By fine mapping sex differences in subcortical maturation, we find that significant sex differences in the timing of overall volume change within the developing striatum (male delay), pallidum (trend toward female delay), and thalamus (male delay) are accompanied by regionally specific rather than global sex differences in maturation. Our localization of sexually dimorphic subcortical maturation informs the future study of sex-biased mental disorders.

Our study encompasses the adolescent transition into early adulthood, during which females develop a greater risk for affective disorders than males and males show a greater surge in risk-taking and antisocial behavior relative to females (35, 36). We find that during this same developmental window, males and females also show growing anatomical dissimilarities within several subcortical regions implicated in the neurobiology of such conditions. For example, male and female adolescents show divergent structural maturation within (*i*) ventro-rostral putamen, medial rostral caudate, rostral pallidum, and lateral-dorsal (LD)/MD thalamic foci of functional abnormalities in depression (38) and (*ii*) ventral striatal systems involved in key facets of risk-taking behavior such as inhibitory control, sensation seeking, and reward processing (25, 39). These hotspots of sexually dimorphic striatal, pallidal, and thalamic maturation represent candidate substrates for adolescent-emergent sex differences in liability to disorders of mood and behavioral control—especially when considered alongside recent longitudinal structural neuroimaging evidence for co-occurring sex differences in the structural maturation of prefrontal systems that interact with the subcortex during affect and impulse regulation (34). Further unraveling the relationship between subcortical development and sex differences in adolescent psychopathology will require large-scale longitudinal studies capable of simultaneously capturing individual-level changes in behavior alongside changes in brain structure and function across adolescence. Endocrine data will be critical to such future work given (*i*) close links between pubertal development and subcortically mediated behaviors (72), (*ii*) the puberty-dependent emergence of sex differences in circulating gonadal steroids, and (*iii*) evidence that gonadal steroids can exert

regionally specific effects on subcortical systems during human adolescence (73).

Methods

Participants. We included 1,172 structural magnetic imaging brain scans that had been acquired longitudinally on 618 healthy youth aged between 5 and 25 y or age (Table S1). Participants were recruited through local advertisement. The absence of neurological or psychiatric illness was established through completion of a screening questionnaire (Child Behavior Checklist) and a structured diagnostic interview administered by a child psychiatrist (18). Handedness was established using the Physical and Neurological Examination of Soft Signs. All participants had a full-scale intelligence quotient (FSIQ) of greater than 80 as determined using age-appropriate Wechsler Intelligence Scales including WISC-R, WAIS-R, and WASI (11). Socioeconomic status (SES) was quantified using Hollingshead scales. The institutional review board of the National Institutes of Health approved the research protocol used in this study, and written informed consent and assent to participate in the study were obtained from parents and children, respectively.

Neuroimaging. Scans were acquired at 2-yearly intervals. All sMRI scans were T-1 weighted images with contiguous 1.5-mm axial slices and 2.0-mm coronal slices, obtained on the same 1.5-T General Electric Signa scanner using a 3D spoiled-gradient recalled-echo sequence with the following parameters: echo time, 5 ms; repetition time, 24 ms; flip angle 45°; acquisition matrix, 256 × 192; number of excitations, 1; and field of view, 24 cm. All scans used in this study were free of motion artifact as determined by visual inspection.

Subcortical structures were automatically identified using a recently developed segmentation method known as the MAGeT Brain algorithm (17). To summarize the technique, 3D reconstruction of serial histological data for the striatum, pallidum, and thalamus were warped to an MRI-based template (19). The atlases were then customized to a subset of the dataset (30 randomly selected subjects) using a nonlinear transformation estimated in a region-of-interest defined around the subcortical structures (17, 19, 74, 75). This set of subjects then acts as a set of templates to which all other scans are warped. This procedure provides thirty candidate subcortical segmentations for each scan. The final segmentation is decided upon using a voxel-wise majority vote; that is, the label occurring most frequently at a specific location is retained (76). These methods are reliable in comparisons against "gold standard" manual definitions (Dice Kappa = 0.86) (17). A quality control image file is provided for each scan, allowing detailed visual inspection to rule out the presence of segmentation errors (see Fig. S4 for examples of "fail" and "pass" segmentations).

To determine shape, surface-based representations of subcortical structures defined on the input atlas were first estimated using the marching cubes algorithm (16) and then morphologically smoothed using the AMIRA software package (Visage Imaging). Next, the nonlinear portions of the 30 transformations mapping each subject to the 30 input templates were concatenated and averaged across the template library to limit the effects of noise and error and to increase precision and accuracy. These surface-based representations were warped to fit each template, and, as in the case of the segmentation, each of these surfaces was warped to match each subject. This procedure yields thirty possible surface representations per subject that are then merged by creating a new surface representation of the striatum or pallidum by estimating the median coordinate representation at each location. At this point, a third of the surface of each triangle is assigned to each vertex within the triangle. The surface area value stored at each vertex is the sum of all such assignments from all connected triangles. Finally, surface-area values were blurred with a surface-base diffusion-smoothing kernel (5 mm and 3 mm for the striatum/thalamus and pallidum, respectively). The measures of interest generated by this processing stream for each scan were total volume estimates for left and right striatum, pallidum, and thalamus (summed to provide a single estimate of total bilateral volume for each structure) and surface area at a total of 21,156 vertices across all structures (striatum, 6,450 left/6,178 right; pallidum, 1,266 left/1,138 right; thalamus, 3,016 left/3,108 right). To derive measures of cortical volume as a comparison for measures of subcortical volume, we submitted all scans to the previously described CIVET pipeline for automated morphometric analysis (2, 77).

Analysis. ***Gross volumetric development.*** We used mixed models (78) to estimate the fixed effects of age and sex and interactions between these terms on the total bilateral volume of each structure. Two random intercepts modeled variance dependence for person and for person within family. First, to assess the curvilinearity of subcortical volume development in males and females, while allowing trajectories for males and females to vary in shape, we applied F-tests (df = 2) to determine whether the combined contribution of sex and polynomial age terms was significant, using a step-down approach through cubic, quadratic, and linear models. Then, sex differences in the selected trajectory shape we assessed using a Likelihood Ratio test to determine whether a model including interactions between age terms and sex (Eq. **1**) predicted significantly more variance in the measure of interest compared with a simpler model including only age terms and a main effect of sex (Eq. **2**) (i.e., to test whether growth curve "shape" for the structure of interest was significantly different between males and females). Thus, using cubic modeling of striatal volume growth with age as an example, we compared the following two models where striatal volume (SV) at ith family's jth individual's kth time point was modeled as:

$$SV_{ijk} = \text{Intercept} + d_i + d_{ij} + \beta_1(\text{sex}) + \beta_2(\text{age}) + \beta_3(\text{age}^2) + \beta_4(\text{age}^3) + \beta_5(\text{sex} * \text{age}) + \beta_6(\text{sex} * \text{age}^2) + \beta_7(\text{sex} * \text{age}^3) + e_{ijk}. \quad [1]$$

$$SV_{ijk} = \text{Intercept} + d_i + d_{ij} + \beta_1(\text{sex}) + \beta_2(\text{age}) + \beta_3(\text{age}^2) + \beta_4(\text{age}^3) + e_{ijk}. \quad [2]$$

All models were run using "mean-centered" age terms so that the sex-term coefficient refers to the sex effects at mean age (13.11 y) rather than age zero. For those structures that followed nonlinear developmental trajectories, the "age-at-peak" was determined by solving the first-order derivative of the growth trajectory equation defined for that structure. Confidence intervals for trajectories of volume and volume change and the timing of volumetric peaks were derived by bootstrapping methods involving reestimation of model parameters for each of 1,000 resamplings from our participant pool.

Regionally heterochronous subcortical development. At each vertex of each subcortical structure, surface area was first modeled in a manner analogous to that adopted for total volume of each subcortical structure (Eq. **1**). These analyses indicated that, after false discovery rate (FDR) correction for multiple comparisons (41), ∼35% of subcortical vertices showed significant quadratic effects of age whereas linear age effects applied to over 75% of subcortical vertices. We therefore focused on linear age effects when analyzing inter-vertex and male–female differences in regional subcortical surface-area development, and we present findings for regionally quadratic effects of age in Fig. S5. Given the lack of existing information about regional variation in the rate of subcortical maturation, we first derived unthresholded maps for the main effect of linear age at each vertex (i.e., β_1 coefficient in Eq. **2** below, after FDR correction):

$$\text{Vertex\_SA}_{ijk} = \text{Intercept} + d_i + d_{ij} + \beta_1(\text{age}) + e_{ijk}. \quad [3]$$

Next, we identified foci of significant male–female differences in subcortical maturation by deriving thresholded *t*-statistic maps for the interaction between age and sex on vertex surface area (i.e., β_3 coefficient in Eq. **3** below, after FDR correction):

$$\text{Vertex\_SA}_{ijk} = \text{Intercept} + d_i + d_{ij} + \beta_1(\text{sex}) + \beta_2(\text{age}) + \beta_3(\text{sex} * \text{age}) + e_{ijk}. \quad [4]$$

All statistical analyses and data visualizations were conducted using the R language for statistical computing (79–81).

1. Giedd JN, Rapoport JL (2010) Structural MRI of pediatric brain development: what have we learned and where are we going? *Neuron* 67(5):728–734.
2. Raznahan A, et al. (2011) How does your cortex grow? *J Neurosci* 31(19):7174–7177.
3. Gilmore JH, et al. (2012) Longitudinal development of cortical and subcortical gray matter from birth to 2 years. *Cereb Cortex* 22(11):2478–2485.
4. Tamnes CK, et al.; Alzheimer's Disease Neuroimaging Initiative (2013) Brain development and aging: Overlapping and unique patterns of change. *Neuroimage* 68:63–74.
5. Gogtay N, et al. (2004) Dynamic mapping of human cortical development during childhood through early adulthood. *Proc Natl Acad Sci USA* 101(21):8174–8179.
6. Hughes EJ, et al. (2012) Regional changes in thalamic shape and volume with increasing age. *Neuroimage* 63(3):1134–1142.
7. Koikkalainen J, et al. (2007) Shape variability of the human striatum: Effects of age and gender. *Neuroimage* 34(1):85–93.
8. Ostby Y, et al. (2009) Heterogeneity in subcortical brain development: A structural magnetic resonance imaging study of brain maturation from 8 to 30 years. *J Neurosci* 29(38):11772–11782.
9. Brain Development Cooperative Group (2012) Total and regional brain volumes in a population-based normative sample from 4 to 18 years: The NIH MRI Study of Normal Brain Development. *Cereb Cortex* 22(1):1–12.

10. Hill J, et al. (2010) Similar patterns of cortical expansion during human development and evolution. *Proc Natl Acad Sci USA* 107(29):13135–13140.
11. Shaw P, et al. (2006) Intellectual ability and cortical development in children and adolescents. *Nature* 440(7084):676–679.
12. Vidal CN, et al. (2006) Dynamically spreading frontal and cingulate deficits mapped in adolescents with schizophrenia. *Arch Gen Psychiatry* 63(1):25–34.
13. Shaw P, Gogtay N, Rapoport J (2010) Childhood psychiatric disorders as anomalies in neurodevelopmental trajectories. *Hum Brain Mapp* 31(6):917–925.
14. Parent A, Hazrati LN (1995) Functional anatomy of the basal ganglia. I. The cortico-basal ganglia-thalamo-cortical loop. *Brain Res Brain Res Rev* 20(1):91–127.
15. Reiner A, Medina L, Veenman CL (1998) Structural and functional evolution of the basal ganglia in vertebrates. *Brain Res Brain Res Rev* 28(3):235–285.
16. Lerch JP, et al. (2008) Automated deformation analysis in the YAC128 Huntington disease mouse model. *Neuroimage* 39(1):32–39.
17. Mallar Chakravarty M, et al. (2012) Performing label-fusion-based segmentation using multiple automatically generated templates. *Hum Brain Mapp* 34(10):2635–2654.
18. Giedd JN, et al. (1999) Brain development during childhood and adolescence: A longitudinal MRI study. *Nat Neurosci* 2(10):861–863.
19. Chakravarty MM, Bertrand G, Hodge CP, Sadikot AF, Collins DL (2006) The creation of a brain atlas for image guided neurosurgery using serial histological data. *Neuroimage* 30(2):359–376.
20. Schaltenbrand G, Wahren W (1977) *Atlas for Stereotaxy of the Human Brain* (Georg Thieme Verlag, Stuttgart, Germany).
21. Hirai T, Jones EG (1989) A new parcellation of the human thalamus on the basis of histochemical staining. *Brain Res Brain Res Rev* 14(1):1–34.
22. Shaw P, et al. (2008) Neurodevelopmental trajectories of the human cerebral cortex. *J Neurosci* 28(14):3586–3594.
23. Lenroot RK, et al. (2007) Sexual dimorphism of brain developmental trajectories during childhood and adolescence. *Neuroimage* 36(4):1065–1073.
24. Fjell AM, et al. (2013) High-expanding cortical regions in human development and evolution are related to higher intellectual abilities. *Cereb Cortex*, 10.1093/cercor/bht201.
25. Padmanabhan A, Geier CF, Ordaz SJ, Teslovich T, Luna B (2011) Developmental changes in brain function underlying the influence of reward processing on inhibitory control. *Dev Cogn Neurosci* 1(4):517–529.
26. Casey B, Jones RM, Somerville LH (2011) Braking and accelerating of the adolescent brain. *J Res Adolesc* 21(1):21–33.
27. Haber SN, Knutson B (2010) The reward circuit: Linking primate anatomy and human imaging. *Neuropsychopharmacology* 35(1):4–26.
28. Haber SN, Calzavara R (2009) The cortico-basal ganglia integrative network: The role of the thalamus. *Brain Res Bull* 78(2-3):69–74.
29. Redgrave P, et al. (2010) Goal-directed and habitual control in the basal ganglia: Implications for Parkinson's disease. *Nat Rev Neurosci* 11(11):760–772.
30. Draganski B, et al. (2008) Evidence for segregated and integrative connectivity patterns in the human basal ganglia. *J Neurosci* 28(28):7143–7152.
31. Crittenden JR, Graybiel AM (2011) Basal ganglia disorders associated with imbalances in the striatal striosome and matrix compartments. *Front Neuroanat* 5:59.
32. Zhang D, Snyder AZ, Shimony JS, Fox MD, Raichle ME (2010) Noninvasive functional and structural connectivity mapping of the human thalamocortical system. *Cereb Cortex* 20(5):1187–1194.
33. Sowell ER, et al. (2003) Mapping cortical change across the human life span. *Nat Neurosci* 6(3):309–315.
34. Raznahan A, et al. (2010) Longitudinally mapping the influence of sex and androgen signaling on the dynamics of human cortical maturation in adolescence. *Proc Natl Acad Sci USA* 107(39):16988–16993.
35. Statistics FIFoCaF (2009) *America's Children: Key National Indicators of Well-Being* (US Government Printing Office, Washington, DC).
36. Green H, McGinnity A, Meltzer H, Ford T, Goodman R (2004) *Mental Health of Children and Young People in Great Britain, 2004* (Palgrave Macmillan, Basingstoke, UK).
37. Forbes EE, Dahl RE (2012) Research review: Altered reward function in adolescent depression: What, when and how? *J Child Psychol Psychiatry* 53(1):3–15.
38. Diener C, et al. (2012) A meta-analysis of neurofunctional imaging studies of emotion and cognition in major depression. *Neuroimage* 61(3):677–685.
39. Glenn AL, Yang Y (2012) The potential role of the striatum in antisocial behavior and psychopathy. *Biol Psychiatry* 72(10):817–822.
40. Schneider S, et al.; IMAGEN Consortium (2012) Risk taking and the adolescent reward system: A potential common link to substance abuse. *Am J Psychiatry* 169(1):39–46.
41. Genovese CR, Lazar NA, Nichols T (2002) Thresholding of statistical maps in functional neuroimaging using the false discovery rate. *Neuroimage* 15(4):870–878.
42. Gasser T, Molinari L, Largo R (2013) A comparison of pubertal maturity and growth. *Ann Hum Biol* 40(4):341–347.
43. Marshall WA, Tanner JM (1969) Variations in pattern of pubertal changes in girls. *Arch Dis Child* 44(235):291–303.
44. Marshall WA, Tanner JM (1970) Variations in the pattern of pubertal changes in boys. *Arch Dis Child* 45(239):13–23.
45. Finlay BL, Darlington RB (1995) Linked regularities in the development and evolution of mammalian brains. *Science* 268(5217):1578–1584.
46. Laird AR, et al. (2011) Behavioral interpretations of intrinsic connectivity networks. *J Cogn Neurosci* 23(12):4022–4037.
47. Ferry AT, Ongür D, An X, Price JL (2000) Prefrontal cortical projections to the striatum in macaque monkeys: Evidence for an organization related to prefrontal networks. *J Comp Neurol* 425(3):447–470.
48. McFarland NR, Haber SN (2001) Organization of thalamostriatal terminals from the ventral motor nuclei in the macaque. *J Comp Neurol* 429(2):321–336.
49. Selemon LD, Goldman-Rakic PS (1990) Topographic intermingling of striatonigral and striatopallidal neurons in the rhesus monkey. *J Comp Neurol* 297(3):359–376.
50. Giguere M, Goldman-Rakic PS (1988) Mediodorsal nucleus: Areal, laminar, and tangential distribution of afferents and efferents in the frontal lobe of rhesus monkeys. *J Comp Neurol* 277(2):195–213.
51. Cohen MX, Schoene-Bake JC, Elger CE, Weber B (2009) Connectivity-based segregation of the human striatum predicts personality characteristics. *Nat Neurosci* 12(1):32–34.
52. Leh SE, Ptito A, Chakravarty MM, Strafella AP (2007) Fronto-striatal connections in the human brain: A probabilistic diffusion tractography study. *Neurosci Lett* 419(2):113–118.
53. Behrens TE, et al. (2003) Non-invasive mapping of connections between human thalamus and cortex using diffusion imaging. *Nat Neurosci* 6(7):750–757.
54. Chikama M, McFarland NR, Amaral DG, Haber SN (1997) Insular cortical projections to functional regions of the striatum correlate with cortical cytoarchitectonic organization in the primate. *J Neurosci* 17(24):9686–9705.
55. DeVito JL, Anderson ME, Walsh KE (1980) A horseradish peroxidase study of afferent connections of the globus pallidus in Macaca mulatta. *Exp Brain Res* 38(1):65–73.
56. Hazrati LN, Parent A (1992) The striatopallidal projection displays a high degree of anatomical specificity in the primate. *Brain Res* 592(1-2):213–227.
57. Giménez-Amaya JM, McFarland NR, de las Heras S, Haber SN (1995) Organization of thalamic projections to the ventral striatum in the primate. *J Comp Neurol* 354(1):127–149.
58. Kuo JS, Carpenter MB (1973) Organization of pallidothalamic projections in the rhesus monkey. *J Comp Neurol* 151(3):201–236.
59. Sidibé M, Bevan MD, Bolam JP, Smith Y (1997) Efferent connections of the internal globus pallidus in the squirrel monkey. I. Topography and synaptic organization of the pallidothalamic projection. *J Comp Neurol* 382(3):323–347.
60. Ray JP, Price JL (1993) The organization of projections from the mediodorsal nucleus of the thalamus to orbital and medial prefrontal cortex in macaque monkeys. *J Comp Neurol* 337(1):1–31.
61. Xiao D, Zikopoulos B, Barbas H (2009) Laminar and modular organization of prefrontal projections to multiple thalamic nuclei. *Neuroscience* 161(4):1067–1081.
62. Schmahmann JD, Pandya DN (1990) Anatomical investigation of projections from thalamus to posterior parietal cortex in the rhesus monkey: A WGA-HRP and fluorescent tracer study. *J Comp Neurol* 295(2):299–326.
63. Cappe C, Morel A, Rouiller EM (2007) Thalamocortical and the dual pattern of corticothalamic projections of the posterior parietal cortex in macaque monkeys. *Neuroscience* 146(3):1371–1387.
64. Sadikot AF, Rymar VV (2009) The primate centromedian-parafascicular complex: Anatomical organization with a note on neuromodulation. *Brain Res Bull* 78(2-3):122–130.
65. Parvizi J, Van Hoesen GW, Buckwalter J, Damasio A (2006) Neural connections of the posteromedial cortex in the macaque. *Proc Natl Acad Sci USA* 103(5):1563–1568.
66. Leichnetz GR (2001) Connections of the medial posterior parietal cortex (area 7m) in the monkey. *Anat Rec* 263(2):215–236.
67. Middleton FA, Strick PL (1996) The temporal lobe is a target of output from the basal ganglia. *Proc Natl Acad Sci USA* 93(16):8683–8687.
68. Webster MJ, Bachevalier J, Ungerleider LG (1993) Subcortical connections of inferior temporal areas TE and TEO in macaque monkeys. *J Comp Neurol* 335(1):73–91.
69. Brand S, Rakic P (1984) Cytodifferentiation and synaptogenesis in the neostriatum of fetal and neonatal rhesus monkeys. *Anat Embryol (Berl)* 169(1):21–34.
70. Paus T, et al. (1999) Structural maturation of neural pathways in children and adolescents: In vivo study. *Science* 283(5409):1908–1911.
71. Gogtay N, et al. (2008) Three-dimensional brain growth abnormalities in childhood-onset schizophrenia visualized by using tensor-based morphometry. *Proc Natl Acad Sci USA* 105(41):15979–15984.
72. Forbes EE, Dahl RE (2010) Pubertal development and behavior: Hormonal activation of social and motivational tendencies. *Brain Cogn* 72(1):66–72.
73. Op de Macks ZA, et al. (2011) Testosterone levels correspond with increased ventral striatum activation in response to monetary rewards in adolescents. *Dev Cogn Neurosci* 1(4):506–516.
74. Chakravarty MM, et al. (2009) Comparison of piece-wise linear, linear, and nonlinear atlas-to-patient warping techniques: Analysis of the labeling of subcortical nuclei for functional neurosurgical applications. *Hum Brain Mapp* 30(11):3574–3595.
75. Chakravarty MM, Sadikot AF, Germann J, Bertrand G, Collins DL (2008) Towards a validation of atlas warping techniques. *Med Image Anal* 12(6):713–726.
76. Collins DL, Pruessner JC (2010) Towards accurate, automatic segmentation of the hippocampus and amygdala from MRI by augmenting ANIMAL with a template library and label fusion. *Neuroimage* 52(4):1355–1366.
77. Ad-Dab'bagh Y, et al. (2006) The CIVET image-processing environment: A fully automated comprehensive pipeline for anatomical neuroimaging research. *Proceedings of the 12th Annual Meeting of the Organization for Human Brain Mapping*, ed Corbetta M (Organization for Human Brain Mapping, Minneapolis, MN). Available at http://www.bic.mni.mcgill.ca/users/yaddab/Yasser-HBM2006-Poster.pdf.
78. Pinheiro J, Bates D (2000) *Mixed-Effects Models in S and S-PLUS* (Springer, New York).
79. R Core Team (2013) R: A language and environment for statistical computing (R Foundation for Statistical Computing, Vienna).
80. Wickham H (2009) *ggplot2: Elegant Graphics for Data Analysis* (Springer, New York).
81. Pinheiro J, Bates D, DebRoy S, Sarkar D, R Development Core Team (2013) nlme: Linear and Nonlinear Mixed Effects Models. R package version 3.1-108.